ACTA IMEKO
ISSN: 2221-870X
June 2024, Volume 13, Number 2, 1 - 7

Developing a quantitative multimodal and multi-scale, fully non-destructive technique for the study of iron archaeological artefacts

Elodie Granget[1], Ocson Cocen[1,2], Mahdieh Shakoorioskooie [3], Qianru Zhan[3,4], Marian Nida Lumongsod-Thompson[2], Anders Kaestner[3], David Mannes[3], Laura Brambilla[1]

[1] *Haute Ecole Arc Conservation-restauration, HES-SO University of Applied Sciences and Arts Western Switzerland, Espace de l'Europe 11, 2000 Neuchâtel, Switzerland*
[2] *Tribology and Interfacial Chemistry Group, SCI-STI-SM, Institute of Materials, École polytechnique fédérale de Lausanne, Station 12, 1015 Lausanne, Switzerland*
[3] *Laboratory for Neutron Scattering and Imaging at the Paul Scherrer Institute, Forschungsstrasse 111, 5232 Villigen, Switzerland*
[4] *Institute for Building Materials (IfB), ETH Zürich, 8093 Zürich, Switzerland*

ABSTRACT
This article presents the methodology and initial findings of the SNSF Sinergia project CORINT. The project's objective is to elucidate the corrosion mechanisms affecting iron-based structures entrapped in various porous media. This paper focuses specifically on iron archaeological artefacts (IAAs) in soil. A novel multimodal quantitative imaging technique, which integrates neutron and X-ray computed tomography (NX-CT), is under development for non-destructive examination of corrosion processes. The method involves registering and fusing neutron and X-ray tomography data, followed by Gaussian mixture model (GMM) clustering for phase segmentation. Imaging was conducted on two IAAs, *Vrac C* and *BdC1*. Additionally, random cross-sections of these samples underwent analysis through optical microscopy, µRaman spectroscopy, and SEM-EDS to characterize and correlate corrosion layers with NX-CT results. This study yields valuable insights into the corrosion of IAAs, enabling the non-destructive investigation of corrosion processes in porous media. The implications extend beyond the preservation of cultural heritage, to the examination of long-term corrosion behaviors in contemporary iron structures, steel within concrete, and nuclear waste disposal plans.

Section: RESEARCH PAPER

Keywords: Iron corrosion; non-destructive; multimodal analysis; neutron CT; X-ray CT; Raman; SEM-EDS

Citation: E. Granget, O. Cocen, M. Shakoorioskooie, Q. Zhan, M. N. Lumongsod-Thompson, A. Kaestner, D. Mannes, L. Brambilla, Developing a quantitative multimodal and multi-scale, fully non-destructive technique for the study of iron archaeological artefacts, Acta IMEKO, vol. 13 (2024) no. 2, pp. 1-7. DOI: 10.21014/actaimeko.v13i2.1799

Section Editor: Fabio Leccese, Università Degli Studi Roma Tre, Rome, Italy

Received February 28, 2024; **In final form** April 18, 2024; **Published** June 2024

Funding: This work was supported by the Swiss National Science Foundation (SNSF), project number CRSII5_205883 / 1.

Corresponding author: Elodie Granget, e-mail: elodie.granget@he-arc.ch

1. INTRODUCTION

The CORINT project is a Swiss National Science Foundation Sinergia funded research (project number CRII5_205883/1). The primary objectives are to better understand, and address issues related to corrosion phenomena affecting iron objects surrounded by diverse porous media. This project is a collaboration among researchers from the Department of Materials Science and Engineering at the Swiss Federal Institute of Technology in Lausanne (EPFL SCI-STI-SM), the Department of Civil, Environment and Geomatic Engineering at the Swiss Federal Institute of Technology in Zürich (ETHZ BAUG), the Research Unit in Conservation-Restoration of the University of Applied Sciences Arc of Neuchâtel (HE-Arc), and the Laboratory for Neutron Scattering and Imaging at Paul Scherrer Institut (PSI-LNS). In the scope of this project, HE-Arc focuses specifically on Iron Archaeological Artefacts (IAA).

Comprehending the corrosion of IAAs is imperative in the formulation of appropriate conservation and restoration strategies [1]. The natural long-term corrosion that occurred on

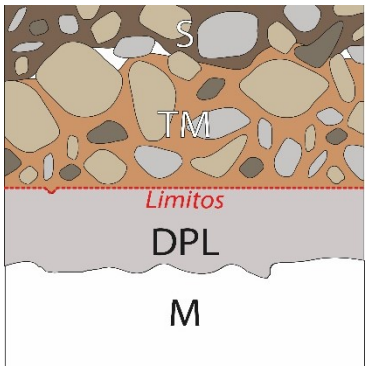

Figure 1. Scheme of stratigraphy of a corroded metallic artefact with each layer designation code.

IAAs makes them not only valuable cultural heritage objects, but also serves as analogues in studies exploring the enduring corrosion patterns of modern iron structures and within nuclear waste disposal plans [2]-[5]. The limitations of laboratory simulations in capturing real-world complexities spanning centuries or millennia underscore the value of IAAs in these investigations. Hence, numerous studies have examined IAAs under various conditions, such as exposure to the atmosphere [6]-[9], burial in various aggressive inland and marine environments [3], [5], [10], [11] and proposed corrosion mechanism models specific to each environment.

In archaeological context, the corrosion processes typically result in the formation of distinct layers. According to convention [3], [12], these layers, from the core outwards, are designated as follows (Figure 1):

- **M** represents the remaining metal core.
- **DPL** signifies the dense product layer located near the metal core. These corrosion products (CP) are produced by mineralization of the object and can still contain technological information such as partial grain structure.
- **Limitos** is the original surface of the object and can still contain traces of fabrication and use. When conservators remove concretions and corrosions from an archaeological artefact, they aim to retrieve this surface [12].
- **TM** designates transformed medium developed above the Limitos of the object, where CP bind with soil sediments and other external markers (i.e., mineralized wood, fabric).
- **S** denotes the layer in which mostly/only sediment (soil for inland archaeology) is present. This equates to the burial medium.

The high reactivity observed in post-excavation IAA, mainly attributed to the presence of compounds like $FeCl_2$ in solution within pores, cracks, and trapped in certain corrosion products (such as akagaeneite), has been a long-standing concern [13]. Nevertheless, the studies that described the corrosion mechanisms employed invasive and destructive analysis methods, possibly causing unwanted changes in these highly reactive objects. Furthermore, acknowledging the inherent scientific and cultural significance of archaeological artefacts underscores the exceptional nature of resorting to invasive analytical techniques, typically limited to more easily obtainable and "sacrificial" objects such as nails. Therefore, examining various iron artefacts and observing them in a truly undisturbed state necessitates the application of a genuinely non-invasive and non-destructive analysis technique. In that regard, the development of techniques such as X-ray tomography [14], [15], neutron tomography [16], and combined X-ray and neutron tomography [17], [18], facilitates the reliable characterization of archaeological artefacts. The latter technique has proven to be an adequate method for the investigation of iron corrosion products.

Hence, a multimodal and quantitative imaging technique based on neutron and X-ray computed tomography (NX-CT) is being developed through the collaborative effort of all partners within the CORINT project. PSI and HE-Arc are working closely to optimize the method for the study of IAAs. The goal is to perform non-destructive quantitative analysis and characterize their corrosion products through Machine Learning-supported segmentation and labelling of all phases identifiable on the neutron and X-ray fused tomograms (NXF). Developing this method implies the use of traditional and invasive analytical techniques, the results of which serve as training data for the Machine Learning model. Once the quantitative multimodal imaging is fully established, it will facilitate the documentation of the initial corrosion state of IAAs in their original surrounding soils. Consequently, this tool will be paramount during laboratory experiments aimed at triggering and documenting changes that would occur during excavation, handling, conservation treatments, such as dechlorination, and storage.

This paper will first present the workflow through which this quantitative NX-CT imaging technique is being developed and optimized for the study of archaeological artefacts. The material and methods for data acquisition are specified and the data obtained on test-objects are discussed. Finally, the remaining development steps of the workflow are summarized in the conclusion.

2. MATERIAL AND METHODS

2.1. Selected objects

A set of iron nails, on which destructive analysis was possible, was provided by the Roman Sites and Museum of Avenches (SMRA), Switzerland, to develop this workflow. In this article, we present the results obtained on *Vrac C* and *BdC1*.

Vrac C is a decontextualized nail that was found in the excavated soil pile by the detectorists alongside others. Since it was not attributed to any stratum, it had low archaeological value and was only partially micro-sandblasted to allow archaeologists to identify its shape. It was then stored in an unmonitored environment and showed signs of chloride presence in the remaining corrosion products.

BdC1 is the first artefact sampled on-site for the CORINT project. It was extracted from the ground during a site survey and kept as a test sample for the NX-CT calibration, as it was already disturbed from its initial environment.

2.2. Workflow

For the development of NX-CT, a sequential data fusion approach was adopted. Initially, neutron and X-ray tomograms are captured at the PSI facility. Subsequently, these tomograms are registered together using an affine transform (SimpleElastix library [19]). The tomograms are then fused and segmented. After image acquisition, the objects are embedded in resin, cut into at least four cross-sections, and studied using optical microscopy (OM), μRaman, and SEM-EDS. The developed workflow aiming at reaching quantitative multimodal imaging involves the training of a Machine Learning model to extrapolate information corresponding to the destructive techniques (2D) using tomography data (2D slice and 3D volume). To make it more robust, calibration material in the form of loose powders

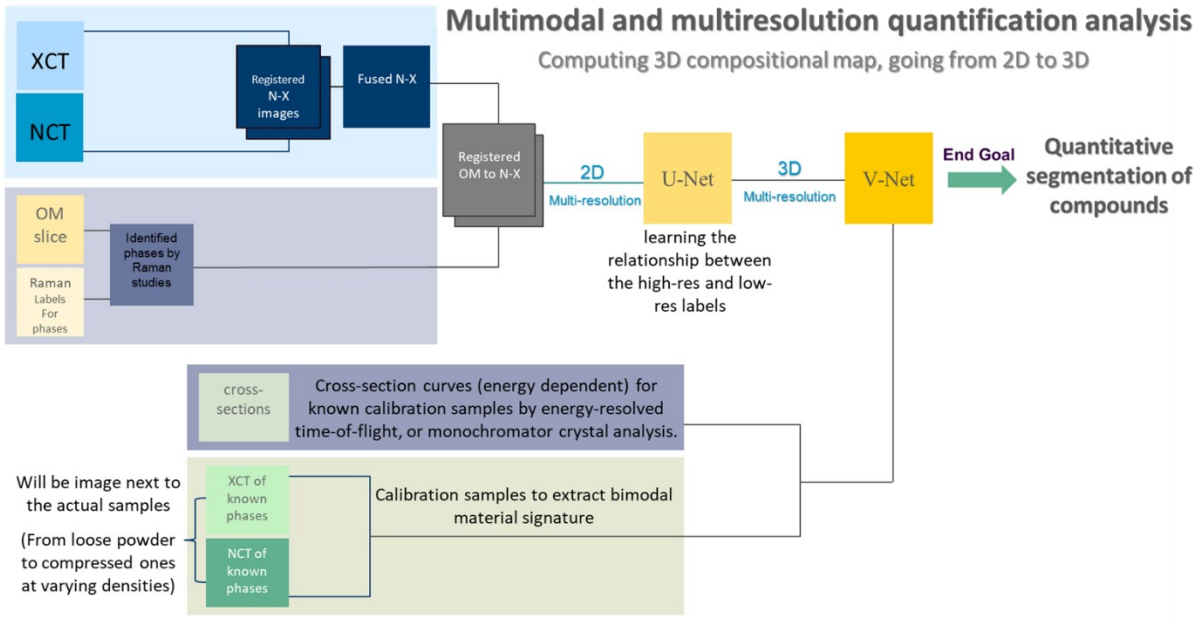

Figure 2. Multimodal quantitative imaging workflow: Converging steps of Data fusion, subsequent training of the ML model with labelled OM images and reference powders. Extrapolation of chemical information to the entire volume.

and pellets of pure corrosion products will provide additional training data. Imaged alongside all studied samples, they will serve as reference points.

Eventually, the trained model will be able to characterize other objects without the need for invasive analysis (Figure 2). This paper discussed in detail the acquisition and data processing steps for the tomograms and cross-section analysis for *Vrac C* and *BdC1*.

2.3. Tomography

Vrac C was mounted on a rotary stand and imaged in ambient air. The tomograms were obtained using a micro-setup at the ICON beamline [20], which employs a cold neutron source and offers higher pixel resolution. Conversely, *BdC1* was first reburied in a Ø5 cm cylinder of soil from Bois de Châtel to simulate a real case scenario. The tomograms were acquired using a midi-setup at the NEUTRA beamline [21], employing thermal neutrons. This set up offers a larger field of view, at the price of a lower pixel resolution, allowing for the capture of the entire nail. The imaging parameters for X-rays and neutrons are detailed in Table 1. Since the moisture contained in the soil is highly attenuating to neutrons, the exposure time at NEUTRA for *BdC1* was pre-emptively set higher.

2.4. Cross-section preparation

After acquisition of the tomograms at PSI, the nails were returned to HE-Arc and prepared into 4 cross-sections for optical microscopy, µRaman spectroscopy and SEM-EDS mapping. They were entirely embedded in EpoFix resin from Struers GmbH, cut and polished down to 4000 grain size, always lubricated with pure Ethanol. To avoid contamination, and because no metallographic observations would be done, the samples were not mirror-polished. They were then marked and stored in a vacuumed desiccator supplemented with silica gel and oxygen absorbers.

Table 1. Parameters for imaging at PSI SINQ facilities

Beamline	Neutron exposure (s)	X-ray exposure (s)	X-ray energy (kV)	Projections	Pixel size (µm)	Horizontal field of view (mm)
ICON	80	10	150	1125	13.8	27
NEUTRA	100	20	250	625	34.4	66.6

2.5. Optical Microscopy, µRaman and SEM-EDS

OM overviews of each cross-section were acquired with a Zeiss microscope equipped with an Axiocam 305 colour digital camera. Multiple views at 5x magnification were stitched together using Zeiss ZEN software. Images were taken in bright field (BF) and dark field (DF), as both might reveal different features. BF optical images were also acquired during µRaman analysis. All OM images were converted to grey scale.

The µRaman analyses were performed with the RENISHAW Virsa Raman analyser, equipped with a BF microscope. All spectra were acquired using a 785nm laser. A first investigation of the cross-section was done by point analysis over visually identified phases. Magnifications of 20x (laser point ~2.4 µm) and 50x (laser point ~1.2 µm) were used to focus the laser on isolated phases. Acquisitions were usually made using the following parameters: 1 second, 25-30 accumulations, and energy between 2-6 mW. The data were then processed with the built-in WIRE 5 software. Phase identification was done using the RRuFF database [22].

Then, to increase coverage and datapoints, Raman maps were acquired using the long-distance 20x objective (Laser spot ~2.7 µm) over 8-10 zones of about 1mm² on each cross-section, encompassing all layers of corrosion from the metal core to the resin. The step size between points was 50 µm and the acquisition parameters were 1 second, 10 accumulations and 2 mW of energy. From these analyses, single component colormaps were created for each phase identified with the WIRE 5 software using reference spectra. These colormaps are superimposed over the analysed zone of the OM image. These are preliminary parameters chosen to maximize the number of points and surface of the map while minimizing acquisition time. They can be readjusted if deemed necessary during the U-Net training phase.

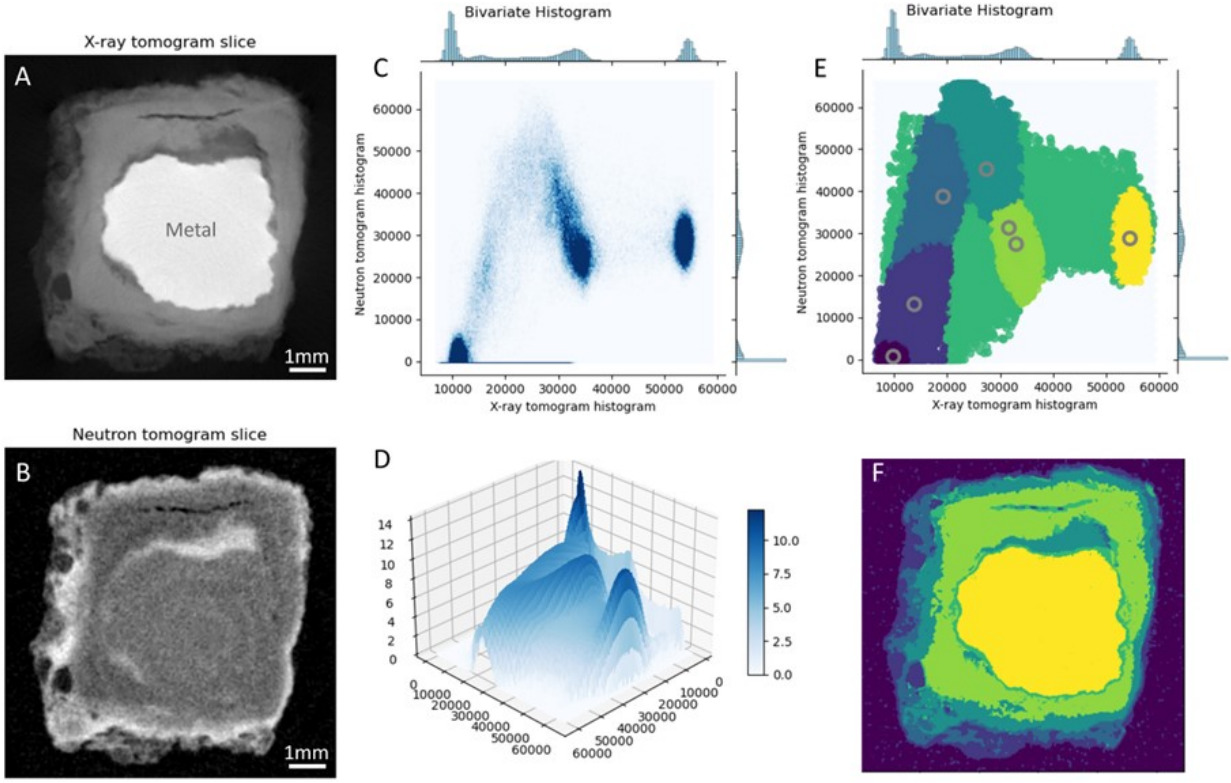

Figure 3. Bimodal imaging and image segmentation results for *Vrac* C sample imaged using ICON instrument at PSI. A. X-ray tomogram slice; B. Neutron tomogram slice; C and D, two- and three-dimensional bivariate histograms of the pixel values based on X-ray and neutron tomograms; E. Clustered bivariate histogram using Gaussian Mixture Model (GMM) with specified priors (grey circles) based on expert opinion; F. Example map of color-coded segmented phases on the corresponding cross-section of the sample, as shown in insets A and B.

In addition to μRaman spectroscopy, SEM-EDS analysis was performed using GeminiSEM 300. SEM images (20 kV, Everhart-Thornley secondary electron detector), EDS spectra (20 kV, 20 s) and EDS maps (20 kV, 40-50 s) were acquired and processed using Aztec software by Oxford Instruments.

3. RESULTS

This section presents the current progress on the developed workflow, namely the CT registration, the characterization of both nails with invasive techniques and the registration of all imaging data.

3.1. CT imaging and registration

The neutron and X-ray images were first reconstructed independently, followed by registration and segmentation using the GMM clustering algorithm based on their bivariate histogram (Figure 3). At this step, the layers can be visually identified by experts, but no chemical or elemental information can be obtained. At time of redaction, the workflow has been fully developed and tested up to data labelling and training of the machine learning model. In the following section, we will describe how the elemental and chemical data are being prepared for accurate labelling in the coming training stage.

3.2. Analysis on cross-sections

The same layers of corrosion identified on the tomograms were found in the object's cross-sections. The characterization of each phase within these layers was done using μRaman point analysis and multiple Raman maps were acquired across the embedded cross-section. Finally, SEM-EDS investigation was performed. This characterization protocol aims at clearly identifying the various layers that were detected and segmented in the NX-CT images and refining the segmentation process, when it appears that some layers were missing or superfluous.

For *Vrac C*, the three main strata, M, DPL, and TM were identified (Figure 4). Phases of the DPL could be analysed with μRaman. TM caused more fluorescence during Raman analysis, probably due to the presence of soil material, making it harder to characterize. A complementary SEM-EDS analysis provided the layers' composition. These analyses revealed elements expected in the soil (Si, Al, Mg, K, Na) [23], mixed with iron oxides.

DPL could be divided into two sub-layers of distinct natures. DPL1 consists of chukanovite (DPL1.1) (Figure 5) [24], with inclusions and reprecipitations of magnetite in fine cracks, displaying signs of rapid re-corrosion at the interface with M. SEM-EDS mapping confirmed the presence of not only Cl- but

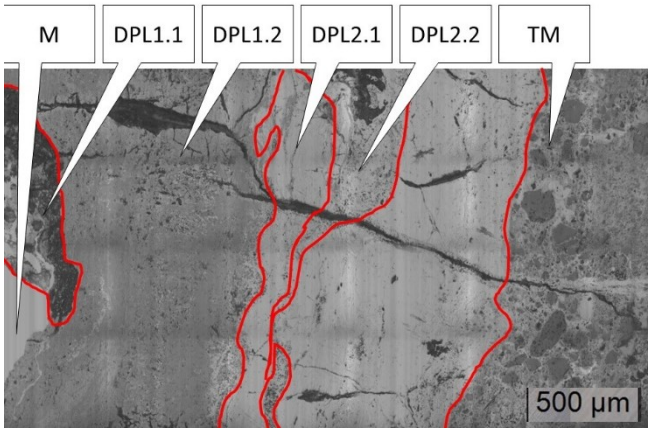

Figure 4. *Vrac* C, bright field OM overview stitched image with main phases as identified with μRaman.

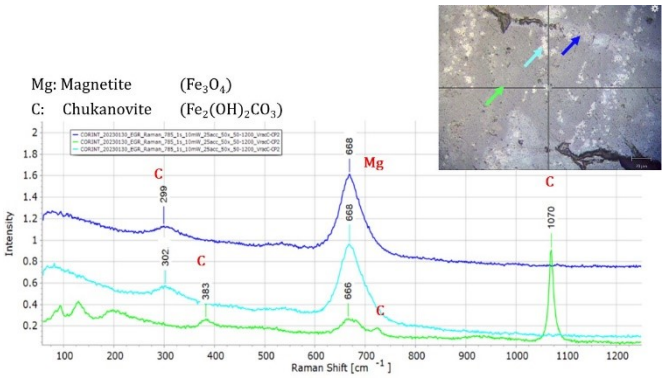

Figure 5. *Vrac* C, µRaman spectra of phases in DPL1.2.

also S-containing phases. DPL2 revealed intermingled phases of magnetite (DPL2.2) and combinations of magnetite and hematite (DPL2.1). Furthermore, all investigated cross-sections exhibited cracks running through all corrosion layers, with reprecipitation phases identified as magnetite, as shown in Figure 5, aligning with expectations from the literature [25]. Cracking was also observed within DPL2 or at the transition between DPL1 and DPL2, leading to clusters of DPL1 within DPL2. µRaman analysis indicated that TM is predominantly composed of a mixture of goethite and akageneite with silicate-based sediments and granite.

BdC1 showed a more complex corrosion pattern (Figure 6). The DPL developed around the nail, under the Limitos, was identified to be a mixture of goethite, magnetite (DPL1) and hematite (DPL2). With the exception of small active corrosion sites containing akageneite, most of this layer is stable (Figure 7A). However, some cross-sections revealed that the nail was partly split open by corrosion (Figure 6B). This corrosion probably progressed along a slag inclusion inside the shank of the nail. There, µRaman analysis revealed a first dense layer of akageneite with magnetite inclusions right at the interface with the remaining metal (DPL1). This layer has multiple cracks. Gradually, the akageneite subsides and a second layer with intertwined phases of magnetite, goethite and hematite with inclusions of siderite can be identified (DPL2). Finally, the outer layer (DPL3) has been identified as lepidocrocite (Figure 7B).

These observations are recorded in the form of a single component colormap for all phases identified in the zones mapped. In addition, single point analyses done at higher magnification are added to ensure small inclusions are also represented in the training data.

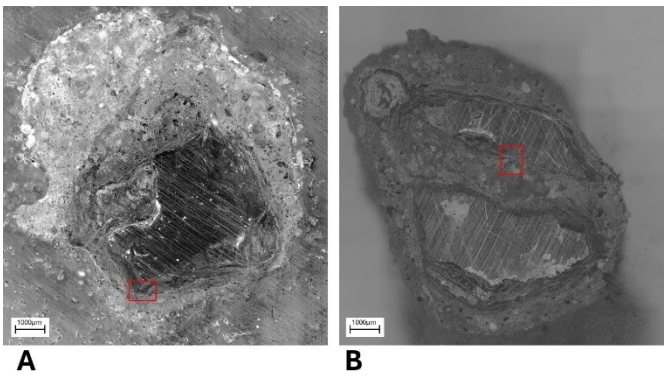

Figure 6. OM overview of two cross-sections of BdC1. Red rectangles showing location of localized map views in Figure 7.

3.3. 2D to 3D registration

The fusion of NXF and the general OM overview plays a crucial role in the preparation for model training. Thus, the OM images of both the general overview and the localized map views of each cross-section were registered (2D to 3D registration) to the corresponding slice in the NXF images (Figure 8 A-D). Along with corresponding Raman map overlays, the localized map views serve as a carrier of chemical information. Essentially, the phase labels are automatically registered, facilitating the fusion with the NXF. A similar procedure will be undertaken between the NXF and SEM images, which carry EDS elemental analysis results. This will aid in identifying elements in the TM, where significant fluorescence has posed challenges in obtaining satisfactory Raman spectra.

Taking multiple cross-sections allows for more accurate extrapolation throughout the tomograms, as it has been shown that a single cross-section cannot be statistically sufficient nor representative of the whole (i.e., *BdC1* inner corrosion). Ultimately, a multimodal fusion of NXF, OM, SEM-EDS, and Raman data will be performed.

4. DISCUSSION

The data acquired through intrusive analysis on *Vrac C* and *BdC1* were processed and interpreted, offering now a better understanding of these two objects. The characterization of the DPL could be performed using µRaman spectroscopy. Difficulties in obtaining good spectra with this technique on TM were solved by completing the analysis with SEM-EDS mapping. The corrosion layers were relatively thick for both nails, and both showed signs of active corrosion that were also identifiable on the fused tomograms. The corrosions found on *BdC1* exemplify perfectly why multiple cross-sections are needed for a more complete and accurate collection of data to feed into the ML model. Indeed, the products found in the corrosion that developed inside the nail shank were of a different nature than the ones in the DPL marking the original surface of the nail.

Regarding the imaging process, the acquisition parameters were optimized, and all registration steps were successful. Even prior to training the ML model, simple observations made on OM cross-sections showed that different features are highlighted by either the NCT, or NXF. Indeed, XCT gives a clear differentiation of the M from the corrosion products (DPL and TM), mostly based on their difference in density. The NCT highlights finer differences within the CP because of the presence of lighter elements such as oxygen and because of moisture content. When combined, the newly fused NX tomograms (NXF) allow for the distinction of active corrosion sites at the M – DPL interface. These first observations were made based on expert opinion and destructive analysis. The

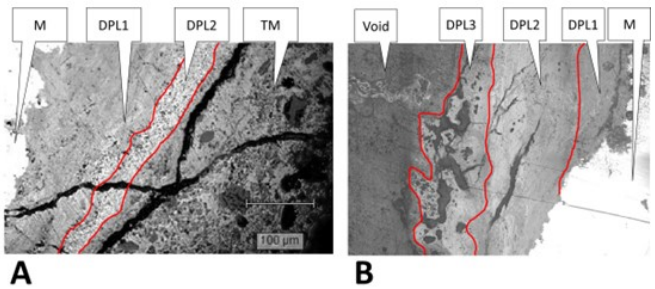

Figure 7. *BdC1* OM for localized map A. Outer corrosion layers. B. Inner corrosion layers.

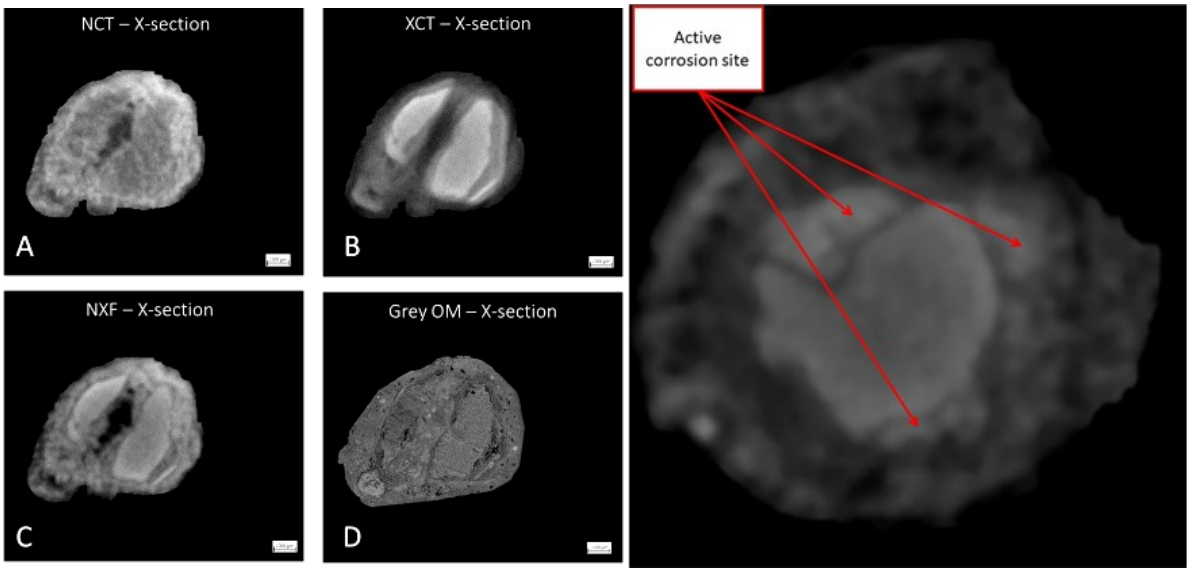

Figure 8. Corresponding slice of registered (A) XCT, (B) NCT, (C) Fused tomograms NXF, and (D) Optical microscopy for Cross-section *BdC1*-d. (E) Other slice of *BdC1* NXF Tomogram, showing active corrosion sites.

coming challenge lies in the accurate labelling and structure of the data that will be used for training the model that should extrapolate the information to other slices as well as to the whole volume on the NXF. This requires a rigorous acquisition of quality data, as well as additional synthetic and augmented data. First Raman maps are being evaluated and their parameters will be revised accordingly. Another critical part will be comprehensively combining Raman chemical data, sufficient for the characterization of the DPL, with EDS elemental data needed for better characterization of the TM.

The cross-referencing of the multi-modal data provides a comprehensive representation of the composition map of the layers identified in the tomograms. To extend the training data, pellets of pure iron oxides and other corrosion products have been produced and are being imaged following the same procedure. This approach paves the way for relying solely on tomography techniques in the future, still providing valuable insights on the nature of corroded iron objects but eliminating the need for destructive sample analyses.

5. CONCLUSION

In conclusion, the development of this multimodal quantitative imaging technique using NX-CT is well underway. This non-destructive approach, attempting the fusion of 3D, 2D, and spectral data, provides valuable insights into the corrosion state of IAAs and offers a promising method for studying corrosion processes in porous media prior to or without extraction from the environment itself.

The results obtained from the analysis of *Vrac C* and *BdC1* demonstrated the effectiveness of the designed workflow. The fusion of neutron and X-ray tomograms enabled the pre-segmentation of different corrosion layers based on clusters identified in their bivariant attenuation histograms. This segmentation will be more precise post-training; optical microscopy, μRaman spectroscopy, and SEM-EDS analysis further contributing to the characterization and labelling. Moving forward, as part of the data augmentation and diversification process, more nails, as well as pure corrosion compounds of iron will be analysed following the same workflow. This diversity will enhance the accuracy of the model.

The ongoing collaboration among project partners and the persistent refinement of the multimodal imaging technique are paving the way for a future reliance solely on tomography techniques. This advancement offers a non-destructive yet comprehensive approach to studying corrosion processes, aligning seamlessly with heritage conservation standards. The results obtained provide conservators and scientists with valuable information to develop tailored conservation treatments, preservation plans, and corrosion mitigation strategies for diverse applications.

Furthermore, the insights derived from the CORINT project transcend the preservation of cultural heritage objects, extending their impact to academia and the materials science industries.

AKNOWLEDGEMENTS

The authors greatly acknowledge the funding by the Swiss National Science Foundation (SNSF), project number CRSII5_205883 / 1

The authors would like to thank the Sites et Musée romains d'Avenches (SMRA), partner of the CORINT project – in particular Myriam Krieg and Pierre Blanc, for providing access to the archaeological sites as well as graciously providing samples for destructive analysis.

REFERENCES

[1] L. Selwyn, Overview of archaeological iron: The corrosion problem, key factors affecting treatment, and gaps in current knowledge, Proc. of Metal 2004: Int. Conf. on Metals Conservation, Canberra, Australia, 2004, pp. 294-306.

[2] W. Miller, Varieties of analogue studies, in: Geological Disposal of Radioactive Wastes and Natural Analogues 2. R. A. W. Miller, N. Chapman, I. Mckinlely, J. Smellie (editors). Pergamon Press, Oxford, 2000, ISBN 0-08-043852-0, pp. 53-63.

[3] D. Neff, P. Dillmann, L. Bellot-Gurlet, G. Beranger, Corrosion of iron archaeological artefacts in soil: characterisation of the corrosion system, Corros. Sci. 47(2) (2005), pp. 515-535. DOI: 10.1016/j.corsci.2004.05.029

[4] W. J. Chitty, P. Dillmann, V. L'Hostis, C. Lombard, Long-term corrosion resistance of metallic reinforcement in concrete—a study of corrosion mechanisms based on archaeological artefacts,

Corros. Sci. 47(6) (2007), pp. 1555-1581.
DOI: doi.org/10.1016/j.corsci.2004.07.032

[5] C. Rémazeilles, D. Neff, J. A. Bourdoiseau, R. Sabot, M. Jeannin, P. Refait, Role of previously formed corrosion product layers on sulfide-assisted corrosion of iron archaeological artefacts in soil, Corros. Sci. 129 (2017), pp. 169-178.
DOI: 10.1016/j.corsci.2017.10.011

[6] P. Dillmann, F. Mazaudier, S. Hoerlé, Advances in understanding atmospheric corrosion of iron. I. Rust characterisation of ancient ferrous artefacts exposed to indoor atmospheric corrosion, Corros. Sci. 46(6) (2004), pp. 1401-1429.
DOI: 10.1016/j.corsci.2003.09.027

[7] S. Hoerlé, F. Mazaudier, P. Dillmann, G. Santarini, Advances in understanding atmospheric corrosion of iron. II. Mechanistic modelling of wet-dry cycles, Corros. Sci. 46(6) (2004), pp. 1431-1465.
DOI: 10.1016/j.corsci.2003.09.028

[8] J. Monnier, E. Burger, P. Berger, D. Neff, I. Guillot, P. Dillmann, Localisation of oxygen reduction sites in the case of iron long term atmospheric corrosion, Corros. Sci. 53(8) (2011), pp. 2468-2473.
DOI: 10.1016/j.corsci.2011.04.002

[9] J. Monnier, D. Neff, S. Réguer, P. Dillmann, L. Bellot-Gurlet, E. Leroy, E. Foy, L. Legrand, (+1 more author), A corrosion study of the ferrous medieval reinforcement of the Amiens cathedral. Phase characterisation and localisation by various microprobes techniques, Corros. Sci. 52(3) (2010), pp. 695-710.
DOI: 10.1016/j.corsci.2009.10.028

[10] F. Mercier-Bion, J. Li, H. Lotz, L. Tortech, D. Neff, P. Dillmann, Electrical properties of iron corrosion layers formed in anoxic environments at the nanometer scale, Corros. Sci. 137 (2018), pp. 98-110.
DOI: 10.1016/j.corsci.2018.03.028

[11] S. Réguer, P. Dillmann, F. Mirambet, Buried iron archaeological artefacts: corrosion mechanisms related to the presence of Cl-containing phases, Corros. Sci. 49(6) (2007), pp. 2726-2744.
DOI: 10.1016/j.corsci.2006.11.009

[12] R. Bertholon, Characterisation and Location of Original Surface of Corroded Metallic Archaeological Objects, Surface Engineering, 17(3) (2001), pp. 241-245.
DOI: 10.1179/026708401101517863

[13] L. S. Selwyn, P. I. Sirois, V. Argyropoulos, The Corrosion of Excavated Archaeological Iron with Details on Weeping and Akaganéite, Studies in Conservation 44(4) (1999), pp. 217–232.
DOI: 10.1179/sic.1999.44.4.217

[14] M. P. Morigi, F. Casali, M. Bettuzzi, R. Brancaccio, V. D'Errico, Application of X-ray computed tomography to cultural heritage diagnostics, Appl. Phys. A. 100(3) (2010), pp. 653–661.
DOI: 10.1007/s00339-010-5648-6

[15] M. Bernabale, F. Cognigni, L. Nigro, M. Rossi, T. De Caro, C. De Vito, A comprehensive strategy for exploring corrosion in iron-based artefacts through advanced Multiscale X-ray Microscopy, Sci. Rep. 12 (2022), p. 6125.
DOI: 10.1038/s41598-022-10151-w

[16] J. Rant, Z. Milič, J. Istenič, T. Knific, I. Lengar, A. Rant, Neutron radiography examination of objects belonging to the cultural heritage, Applied Radiation and Isotopes 64(1) (2006), pp. 7-12.
DOI: 10.1016/j.apradiso.2005.06.003

[17] D. Mannes, F. Schmid, J. Frey, K. Schmidt-Ott, E. Lehmann, Combined neutron and X-ray imaging for non-invasive investigations of cultural heritage objects, Phys. Proc. 69 (2015), pp. 653–660.
DOI: 10.1016/j.phpro.2015.07.092

[18] M. Jacot-Guillarmod, K. Schmidt-Ott, D. Mannes, A. Kaestner, E. Lehmann, C. Gervais, Multi-modal tomography to assess dechlorination treatments of iron-based archaeological artifacts, Herit. Sci. 7 (2019), p. 29.
DOI: 10.1186/s40494-019-0266-x

[19] K. Marstal, F. Berendsen, M. Staring, S. Klein, SimpleElastix: A User-Friendly, Multi-lingual Library for Medical Image Registration, 2016 IEEE Conference on Computer Vision and Pattern Recognition Workshops (CVPRW), Las Vegas, NV, USA, 2016, pp. 574-582.

[20] A. P. Kaestner, S. Hartmann, G. Kühne, G. Frei, C. Grünzweig, L. Josic, F. Schmid, E. H. Lehmann, The ICON beamline – A facility for cold neutron imaging at SINQ, Nuclear Instruments and Methods in Physics Research Section A: Accelerators, Spectrometers, Detectors and Associated Equipment 659(1) (2011), pp. 387-393.
DOI: 10.1016/j.nima.2011.08.022

[21] E. H. Lehmann, P. Vontobel, L. Wiezel, Properties of the Radiography Facility NEUTRA at SINQ and its Potential for Use as European Reference Facility, Nondestructive Testing and Evaluation 16(2-6) (2001), pp. 191-202.
DOI: 10.1080/10589750108953075

[22] B. Lafuente, R. T. Downs, H. Yang, N. Stone, The power of databases: the RRUFF project, in: Highlights in Mineralogical Crystallography, T. Armbruster, R. M. Danisi (editors). W. De Gruyter, Berlin, Germany, 2015, ISBN 9783110417104, pp. 1-30.
DOI: 10.1515/9783110417104-003

[23] G. Sposito, Geochemistry in Soil Science, in: Encyclopedia of Soil Science, W. Chesworth (editor). Encyclopedia of Earth Sciences Series, Springer, Dordrecht, 2008, ISBN 978-1-4020-3994-2.

[24] A. Michelin, Long term alteration of glass/iron systems in anoxic conditions: contribution of archaeological analogues to the study of mechanisms, Thesis in Science des matériaux, Université Pierre et Marie Curie, Paris VI, France, 2011, p. 145.

[25] A. L. Grevey, V. Vignal, H. Krawiec, P. Ozga, K. Peche-Quilichini, A. Rivalan, F. Mazière, Microstructure and long-term corrosion of archaeological iron alloy artefacts, Herit. Sci. 8 (2020), p. 57.
DOI: 10.1186/s40494-020-00398-9